NASA TECHNICAL NOTE

NASA TN D-2923

NASA TN D-2923

FLIGHT EVALUATION OF THE X-15 BALL-NOSE FLOW-DIRECTION SENSOR AS AN AIR-DATA SYSTEM

by John P. Cary and Earl R. Keener

Flight Research Center
Edwards, Calif.

NATIONAL AERONAUTICS AND SPACE ADMINISTRATION • WASHINGTON, D. C. • JULY 1965

NASA TN D-2923

FLIGHT EVALUATION OF THE X-15 BALL-NOSE FLOW-DIRECTION SENSOR AS AN AIR-DATA SYSTEM

By John P. Cary and Earl R. Keener

Flight Research Center
Edwards, Calif.

NATIONAL AERONAUTICS AND SPACE ADMINISTRATION

For sale by the Clearinghouse for Federal Scientific and Technical Information
Springfield, Virginia 22151 – Price $1.00

FLIGHT EVALUATION OF THE X-15 BALL-NOSE FLOW-DIRECTION SENSOR AS AN AIR-DATA SYSTEM

By John P. Cary and Earl R. Keener
Flight Research Center

SUMMARY

27945

An X-15 ball-nose flow-direction sensor was modified to investigate its suitability for air-data measurements of Mach number and pressure altitude. A static-pressure port was added to the nulling sphere at an angle of 70° to the free-stream flow. The static port was calibrated to measure Mach number and pressure altitude in the Mach number range from 0.3 to 5.3 at altitudes up to 130,000 feet and at Reynolds numbers from 0.1 to 1.6 x 10^6 per foot. Dynamic pressure was accurately determined from ball-nose stagnation pressure for Mach numbers up to 5.6 and altitudes up to 180,000 feet.

As shown by this investigation, the capability of the modified flow-direction sensor would probably be limited to Mach numbers less than about 4.5 because of the decreasing sensitivity of the system to changes in Mach number and the increasing influence of nulling error.

For an on-board system, the percentage error in static pressure is approximately twice the percentage error in Mach number, and the calculation of dynamic pressure from ball-nose stagnation pressure can be assumed independent of speed if the free-stream Mach number is greater than 2.5.

Ball-nose lip interference resulted in inaccuracies for a small portion of the flight regime investigated.

author

INTRODUCTION

Air-data parameters such as Mach number and pressure altitude are conveniently determined for most supersonic aircraft by a conventional pitot-static probe. This probe is limited to an angle of attack of 10° or less. Above 10°, the correction of the static-pressure measurements for the effect of angle of attack poses a difficult calibration problem. This problem becomes prohibitive at high supersonic Mach numbers because of the reduced sensitivity of the probe (ref. 1). The conventional probe is also limited structurally because of aerodynamic heating at supersonic speeds.

As a possible solution to the problems resulting from high angle of attack and elevated temperature, an X-15 ball-nose flow-direction sensor was modified to sense Mach number and pressure altitude in addition to angle of attack and sideslip.

This paper assesses the suitability of the modified ball-nose system for obtaining Mach number and pressure altitude from pressure measurements at Mach numbers up to 5.3, altitudes up to 130,000 feet, and Reynolds numbers from 0.1 to 1.6 x 10^6 per foot. The results are compared with experimental and theoretical results for spheres.

Dynamic pressure, calculated from ball-nose stagnation pressure, was compared to the reference system for values up to 1,440 psf. Data are shown for Mach numbers up to 5.6 and altitudes up to 180,000 feet.

SYMBOLS

C_{p_t}	pressure coefficient at the stagnation point
C_{p_θ}	pressure coefficient at angle θ
h_p	pressure altitude above mean sea level, ft
M_∞	free-stream Mach number
p_t	stagnation pressure, psf
p_θ	ball-nose static pressure at angle θ, psf
p_∞	free-stream static pressure, psf
q_∞	free-stream dynamic pressure, psf
α	angle of attack, deg
β	angle of sideslip, deg
γ	ratio of specific heats for air
Δp	differential pressure in angle-of-attack ports, psf
$\epsilon( )$	error in any measured quantity
θ	angle between free-stream flow and the orifice location, deg

Subscripts:

max	maximum

r reference

42°,70°,90° angle between the stagnation-pressure orifice and the static-pressure orifice

X-15 AIRPLANE

The X-15 is a single-place, rocket-powered, research airplane capable of speeds in excess of 6,000 feet per second and altitudes greater than 300,000 feet. It is carried aloft under the wing of a B-52 aircraft and normally launched at an altitude of about 45,000 feet.

A three-view drawing of the X-15 is shown in figure 1, and a detailed description of the airplane is presented in reference 2.

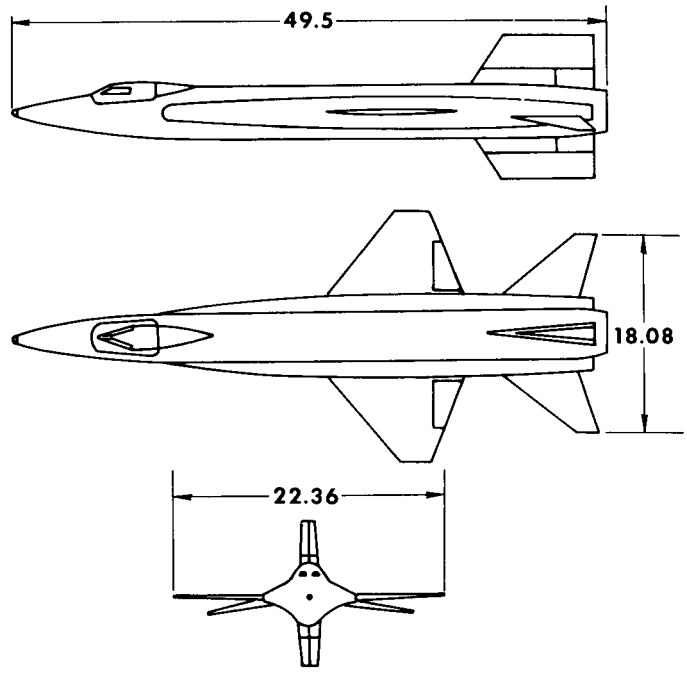

Figure 1.– Three-view drawing of the X-15. All dimensions in feet.

AIR-DATA INSTRUMENTATION

Basic X-15 System

The basic air-data system used in the X-15 flight program is described in detail in reference 3. The reference data sources for free-stream Mach number and dynamic and static pressures in this system are ground radar and rawinsonde instruments sent aloft with weather balloons. The ground radar measures airplane velocity and altitude, and the rawinsonde instruments measure static pressure, static temperature, and winds aloft as a function of altitude. The maximum error in reference free-stream Mach number is estimated to be ±0.06 at $M_{\infty,r} = 2$ and ±0.08 at $M_{\infty,r} = 6$, and the pressure-altitude error is ±1,250 feet at an altitude of 50,000 feet and ±1,500 feet at 100,000 feet.

An on-board air-data system is provided that utilizes a stagnation-pressure measurement just forward of the canopy and a static-pressure measurement from two manifolded orifices, one on each side of the fuselage about 50 inches from the nose. The system is used primarily for subsonic flight, since it is affected by angle of attack at supersonic speeds.

Unmodified Ball-Nose Sensor

The ball-nose flow-direction sensor is a null-seeking, hydraulically actuated, electronically controlled servomechanism designed for operation at elevated temperatures and low dynamic pressures within the X-15 flight envelope. The sphere has four orifices, two in the angle-of-attack plane and two in the angle-of-sideslip plane, for sensing the differential pressure due to α and β. The unbalanced signal from the pressure transducers is fed through amplifiers to the hydraulic actuator, which positions the sphere so as to null the differential pressure. The sphere position relative to the airplane fuselage centerline is indicated and recorded as angle of attack and angle of sideslip. Stagnation pressure at the center orifice is utilized to change the system gain to maintain constant sensitivity throughout the dynamic-pressure range of 15 psf to 2,500 psf. The sphere has a diameter of 6.5 inches and operating ranges from -20° to 40° in angle of attack and ±20° in angle of sideslip. Nulling accuracy from reference 4 is specified as ±0.10° for a free-stream dynamic pressure greater than 30 psf and less than 2,500 psf. The arrangement of the sensors is such that the differential pressures from the transducers cannot be recorded for a direct determination of the nulling accuracy. A more detailed description of the system is presented in reference 4.

Modified Ball-Nose Sensor

For this study, the ball-nose sensor was modified to include a static-pressure orifice at an angle of 70° to the stagnation-pressure orifice. The orifice, as seen in figure 2, is on the upper surface of the sphere so that it rotates away from the lip at the housing junction with increasing angle of attack. The orifice was positioned 27° from the angle-of-attack plane because of structural limitations; however, no adverse effects due to the offset were detected.

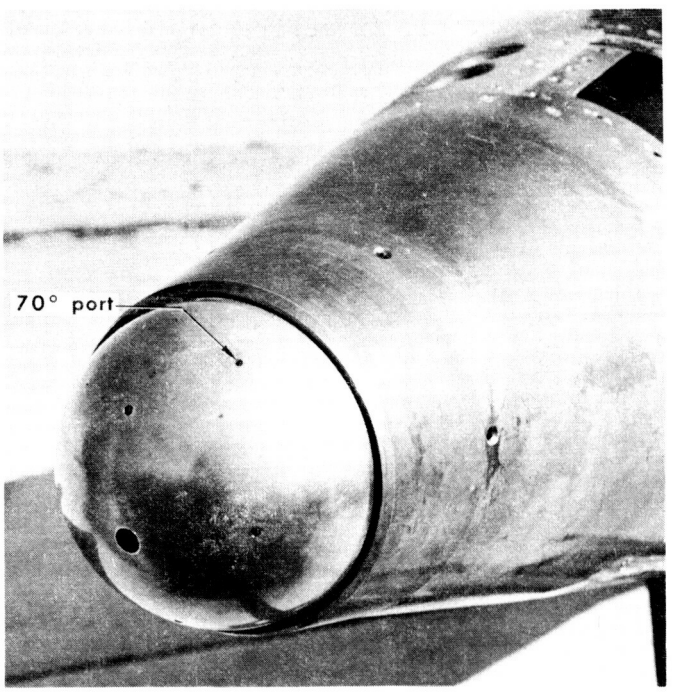

Figure 2.– Photograph of modified ball nose showing the 70° static port.

A schematic drawing of the pressure-sensing and actuator systems is shown in figure 3. The $\theta = 70°$ position was chosen as the best compromise for achieving high sensitivity while eliminating possible interference effects from the lip which extends 5.5° beyond the center of the sphere (fig. 3). At $\alpha = 0°$ and $\beta = 0°$, the angle between the lip and the 70° orifice is 14.5°.

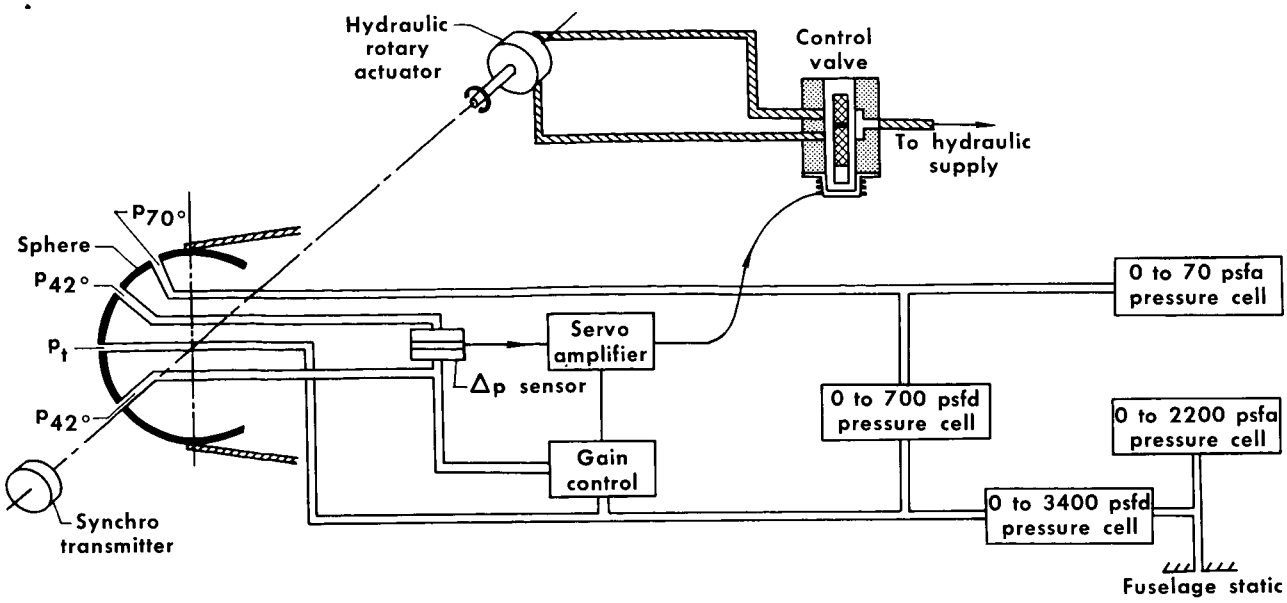

Figure 3.– Schematic drawing of modified flow-direction sensor, showing pressure hookup and actuator system.

Pressure-Recording System

The pressures from the stagnation point p_t, the orifice at $p_{70°}$, and the fuselage static-pressure orifice were recorded on a standard NASA film-recording airspeed-altitude pressure recorder. The recorder has four aneroid-type pressure cells with an estimated accuracy of ±0.5 percent of full scale for the absolute cells and ±0.3 percent of full scale for the differential cells. As shown in figure 3, two high-range cells, one absolute and one differential, with a range from 0 to 2,200 psf and 0 to 3,400 psf, respectively, were used as an internally recorded air-data system. This system is described in reference 3. The absolute cell was connected to the manifolded fuselage static-pressure orifices and the differential cell to the static-pressure orifices and the ball-nose stagnation orifice.

The two remaining low-range cells were used to measure the pressures at the 70° orifice and at the stagnation point. The cells had nominal ranges of 0 to 70 psfa and 0 to 700 psfd, as shown in figure 3. The upper limit of the 0 to 70 psfa cell corresponded to a free-stream dynamic pressure of approximately 250 psf or less. Above this value, $p_{70°}$ was calculated by using the less-accurate high-range cells and the 0 to 700 psfd cell. No data were obtained for a free-stream dynamic pressure greater than about 500 psf, the upper limit of the 0 to 700 psfd cell.

Pressure lag was found to be negligible for the range of pressures in this investigation. Temperature effects on the recording cells were eliminated by calibration.

THEORETICAL CONSIDERATIONS

The method for relating the pressure measurements on a nulling sphere to Mach number and altitude is similar to that used for the standard pitot-static system. The pressure sources are the stagnation pressure p_t from an orifice at the stagnation point of the sphere and the static pressure p_θ from an orifice at some inclination angle θ. As discussed in the following sections, the pressure ratios p_θ/p_t and p_∞/p_θ may be related to Mach number by calibration.

Mach Number and Pressure Altitude

Modified Newtonian theory was used to investigate the variation of the pressures on a nulling sphere for Mach numbers greater than 2. According to the theory, the pressure coefficient at any point θ on the sphere may be determined from the maximum pressure coefficient at the stagnation point as follows

$$C_{p_\theta} = C_{p_t} \cos^2\theta \tag{1}$$

where

$$C_{p_\theta} = \frac{p_\theta - p_\infty}{q_\infty} = \frac{2}{\gamma M_\infty^2}\left(\frac{p_\theta}{p_\infty} - 1\right) \tag{2}$$

and

$$C_{p_t} = \frac{2}{\gamma M_\infty^2}\left(\frac{p_t}{p_\infty} - 1\right) \tag{3}$$

Substituting equations (2) and (3) into equation (1) results in

$$\frac{p_\theta}{p_\infty} - 1 = \frac{p_t}{p_\infty}\cos^2\theta - \cos^2\theta \tag{4}$$

Multiplying by $\frac{p_\infty}{p_t}$ and rearranging terms gives

$$\left.\begin{aligned} \frac{p_\theta}{p_t} &= \frac{p_\infty}{p_t} + \cos^2\theta - \frac{p_\infty}{p_t}\cos^2\theta \\ \frac{p_\theta}{p_t} &= \frac{p_\infty}{p_t}\sin^2\theta + \cos^2\theta \end{aligned}\right\} \tag{5}$$

where

$$\frac{p_t}{p_\infty} = \left[\frac{(\gamma + 1)M_\infty^2}{2}\right]^{\frac{\gamma}{(\gamma-1)}} \left[\frac{(\gamma + 1)}{2\gamma M_\infty^2 - (\gamma - 1)}\right]^{\frac{1}{(\gamma-1)}} \tag{6}$$

Equation (6) is the well-known Rayleigh pitot equation (see ref. 5). Equation (5) is a function of Mach number only, since θ and γ are constant. Static pressure and, in turn, pressure altitude can be determined from equation (4) if Mach number and static pressure at angle θ from the ball nose are known.

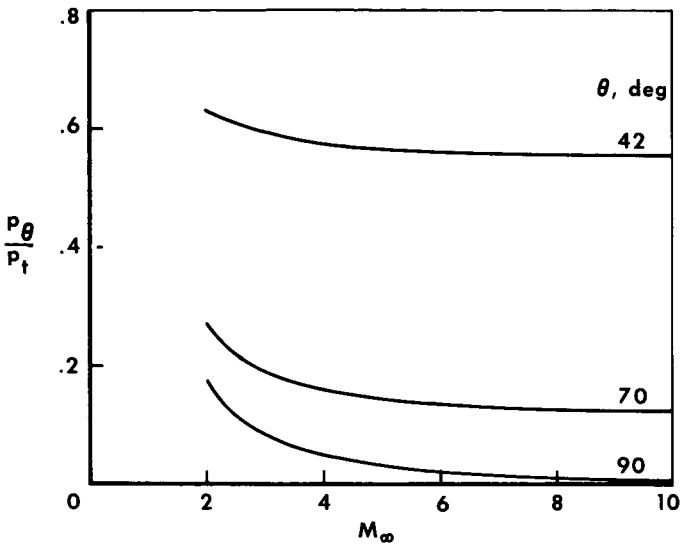

(a) Pressure ratio versus Mach number for several orifice locations.

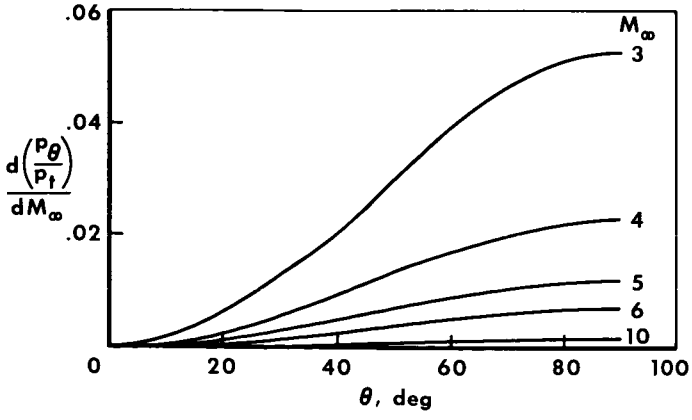

(b) Effect of orifice location on slope of curves in (a).

Figure 4.– Effect of orifice location on measured pressure and accuracy.

The variation of $\frac{p_\theta}{p_t}$ with Mach number as derived from Newtonian theory is shown in figure 4(a) for $\theta = 42°$, (α and β orifice locations on the sphere), 70°, and 90°. According to the theory, $p_{90°} = p_\infty$, or $\frac{p_\theta}{p_t} = \frac{p_\infty}{p_t}$, for a 90° orifice location. As illustrated in figure 4(b), the sensitivity (slope) of the term $\frac{p_\theta}{p_t}$ to changes in Mach number is appreciably affected by orifice position. Thus, the maximum Mach number sensitivity is obtained by positioning the static orifice near $\theta = 90°$. This arrangement is used for the conventional pitot-static probe, which accounts for the superiority of this instrument at low angles of attack. The advantage of orifice position, however, disappears rapidly as Mach number is increased.

Dynamic Pressure

Free-stream dynamic pressure can be determined from the stagnation-pressure measurement on a nulling sphere by using the following equations

$$q_\infty = \frac{\gamma}{2} M_\infty^2 p_\infty \tag{7}$$

$$\frac{q_\infty}{p_t} = \frac{\gamma}{2} M_\infty^2 \frac{p_\infty}{p_t} \tag{8}$$

The term $\frac{p_\infty}{p_t}$ was obtained from the Rayleigh pitot equation (eq. (6)). The quantity $\frac{q_\infty}{p_t}$ is plotted as a function of Mach number in figure 5. This figure shows that $\frac{q_\infty}{p_t}$ increases rapidly with Mach number, reaching a nearly constant value at Mach numbers greater than 3. This characteristic made it possible to provide an on-board presentation of dynamic pressure, as discussed later.

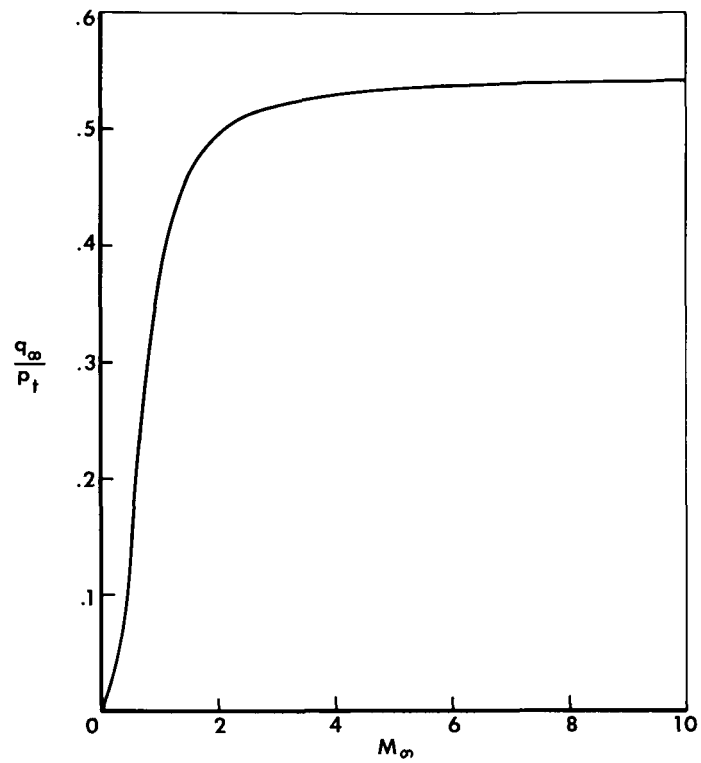

Figure 5.– Ratio of free-stream dynamic pressure to ball-nose stagnation pressure for speeds up to $M_\infty = 10$.

ERROR ANALYSIS

Modified Newtonian theory may also be used to estimate the accuracy of the determinations of free-stream Mach number, static pressure, and dynamic pressure based solely on pressure measurements.

Mach Number

The accuracy in Mach number depends on both the sensitivity of the pressure ratio $\frac{p_\theta}{p_t}$ to M_∞ and the accuracy of the pressure sensors. Thus, the percent error in Mach number may be written in the form

$$\frac{\epsilon(M_\infty)}{M_\infty} = \frac{dM_\infty}{d\left(\frac{p_\theta}{p_t}\right)} \frac{\epsilon\left(\frac{p_\theta}{p_t}\right)\frac{p_\theta}{p_t}}{\frac{p_\theta}{p_t}M_\infty} \tag{9}$$

The Mach number sensitivity $\frac{dM_\infty}{d\left(\frac{p_\theta}{p_t}\right)}$ may be determined from figure 4(b) or the derivative of the Newtonian relationship (eq. (5)). The error in the pressure ratio due to independent and random measurement errors in p_θ and p_t is given by the root-sum-square relation (ref. 6, page 34)

$$\frac{\epsilon\left(\frac{p_\theta}{p_t}\right)}{\frac{p_\theta}{p_t}} = \pm\sqrt{\left[\frac{\epsilon(p_\theta)}{p_\theta}\right]^2 + \left[\frac{\epsilon(p_t)}{p_t}\right]^2} \tag{10}$$

Other possible sources of error in the ball-nose system are nulling inaccuracy, lip effects which are discussed later, and configuration errors of the sphere, such as surface irregularities, or orifice misalinement. Configuration errors are minimized by calibration.

Pressure Altitude

The estimated error in static pressure, which may be related to the error in pressure altitude, may be found from equation (4) as

$$\frac{p_\theta}{p_\infty} - 1 = \frac{p_t}{p_\infty}\cos^2\theta - \cos^2\theta$$

which reduces to

$$p_\infty = \frac{p_\theta}{\sin^2\theta + f(M_\infty)\cos^2\theta}$$

where $f(M_\infty) = \frac{p_t}{p_\infty}$ (eq. (6)). The differential then becomes the error in static pressure

$$\frac{\epsilon(p_\infty)}{p_\infty} = \frac{\epsilon(p_\theta)}{p_\theta} + \frac{f'(M_\infty)\cos^2\theta}{\sin^2\theta + f(M_\infty)\cos^2\theta} \tag{11}$$

where

$$f'(M_\infty) = 7f(M_\infty)\left(\frac{2M_\infty^2 - 1}{7M_\infty^2 - 1}\right)\frac{\epsilon(M_\infty)}{M_\infty} \tag{12}$$

Combining equations (11) and (12) and assuming that M_∞^2 is much greater than 1 and $f(M)\cos^2\theta$ is much greater than $\sin^2\theta$, except when θ approaches 90°, the following expression is obtained

$$\frac{\epsilon(p_\infty)}{p_\infty} \approx \frac{\epsilon(p_\theta)}{p_\theta} + 2\frac{\epsilon(M_\infty)}{M_\infty} \tag{13}$$

The measurement error $\epsilon(p_\theta)$ is known from the recording accuracy of the instrument. The percent Mach number error was derived in the previous section.

Dynamic Pressure

The error in dynamic pressure may be calculated from equation (8), by assuming that Mach number is greater than 3 and

$$\frac{q_\infty}{p_t} = \text{constant}$$

By differentiation

$$\frac{\epsilon(q_\infty)}{q_\infty} = \frac{\epsilon(p_t)}{p_t} \tag{14}$$

Therefore, the error in q_∞ is dependent only on the measurement error of p_t. Below $M_\infty = 3$, Mach number error becomes important because of the slope of the curve calculated by using equation (8) (see fig. 5).

RESULTS AND DISCUSSION

Ball-nose pressure measurements from 10 flights of the X-15 airplane were analyzed. The profiles flown did not allow continuous recording of the pressures from the ball nose because of the dynamic-pressure limit discussed earlier. Overlapping of data from flight to flight eliminated all of the gaps except in the region from $M = 4.20$ to 4.64.

All estimated measurement and nulling errors presented are root-mean-square values.

Mach Number

Calibration.— The calibration curve for Mach number in terms of $\frac{p_{70°}}{p_t}$ versus $M_{\infty,r}$ is shown in figures 6(a) and 6(b).

No subsonic wind-tunnel data are available for comparison with the data of figure 6(a). The results from wind-tunnel tests and modified Newtonian theory are included for comparison at supersonic speeds. The wide scatter in the Mach number range from 0.9 to 1.3 (fig. 6(a)) is believed to be caused by the unsteady shock effects in the vicinity of the ball.

Figure 6(b) shows that the slope of the flight data is generally lower than predicted by Newtonian theory at Mach numbers above 2; however, the theory does not take into account the expansion of the air around the sides of the sphere near a Mach number of 2 or the bluntness effect above a Mach number of 3. Also, the decreasing slope of the curve as Mach number increases should be noted.

Above a Mach number of 3, the flight data are in good agreement with the blunt-body numerical solution given in reference 7. Also, the agreement with wind-tunnel data from reference 8 is good. No effect from variations in Reynolds numbers was found in the flight data.

Measurement error.– The estimated deviation in Mach number with altitude at $M_\infty = 3$ is shown in figure 7(a). The values are based on equation (9) and are typical of any Mach number between 3 and 6. Although this trend may appear to be incorrect, since equation (9) is a function of the error, slope, and magnitude of the pressure ratio, for this study, the factors balanced out to give essentially a constant error with increasing Mach number.

The curves of figure 7(a) also show how staging to the

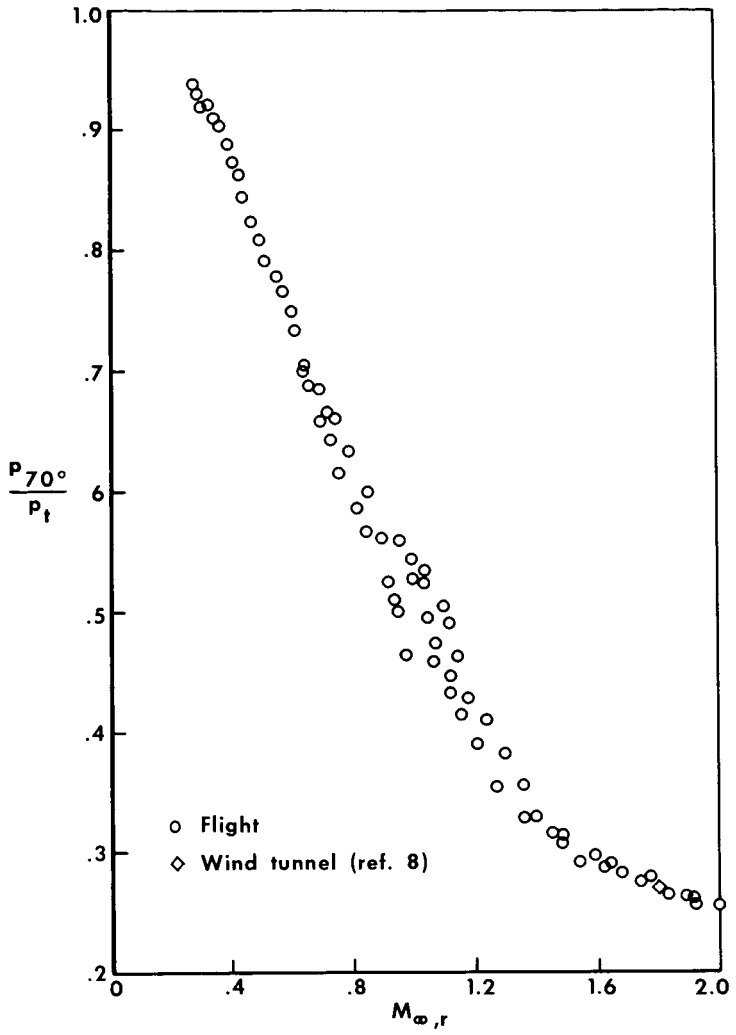

(a) $M_{\infty,r} = 0$ to 2.0.

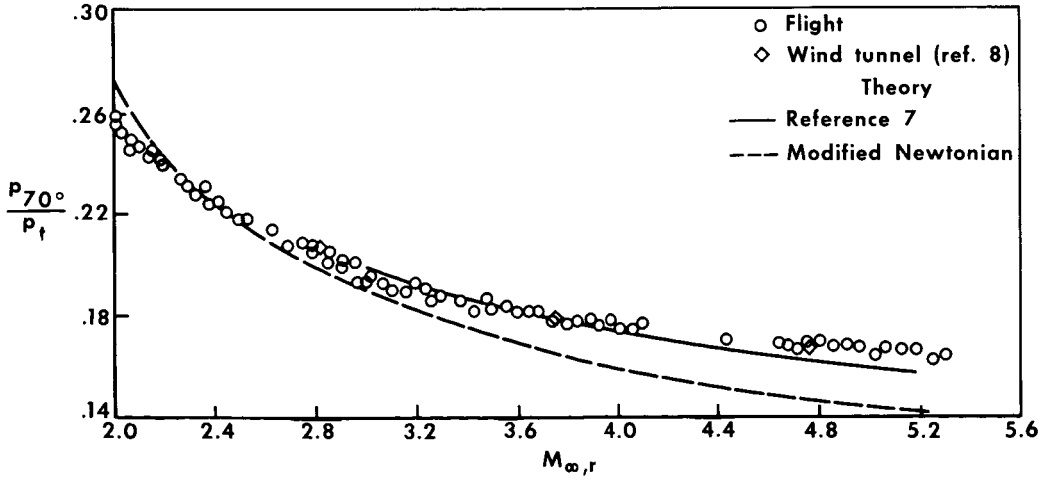

(b) $M_{\infty,r} = 2.0$ to 5.3.

Figure 6.– Calibration of $\frac{p_{70°}}{p_t}$ versus $M_{\infty,r}$ for the X-15 ball nose.

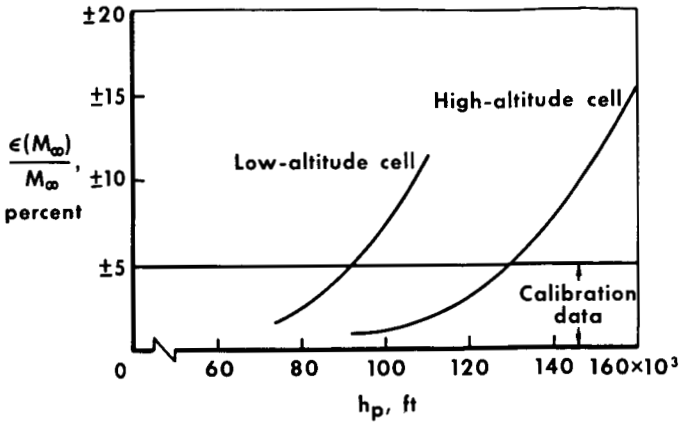

(a) Measurement error for M = 3.

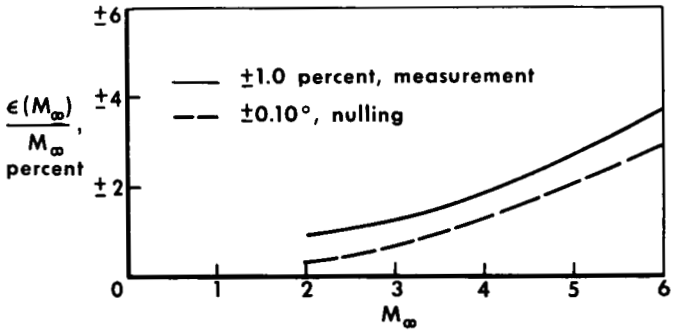

(b) Effect of constant nulling and measurement error.

Figure 7.– Estimated X-15 system errors for $\theta = 70^\circ$.

lower-range cell decreases error. The high-altitude curve begins when the pressure at the 70° orifice falls below the upper limit of the 0 to 70 psfa cell or at about q_∞ = 250 psf. Flight data were not used in the calibration if the estimated Mach number error was greater than ±5 percent.

Figure 7(b) shows the error caused by a ±1 percent measurement error and a ±0.10° nulling error. The measurement-error curve is based on equation (9), as was figure 7(a). However, the measurement error was held constant at ±1 percent so that the effect of slope on the error could be seen. The Mach number error caused by any measurement error can be found easily by multiplying the appropriate value from the curve by the magnitude of the measurement error. For example, at $M_\infty = 4.0$ the estimated error in Mach number is almost ±2 percent. Assuming the measurement error to be on the order of 2 percent to 3 percent, the resulting Mach number error would be 4 percent to 6 percent, a value considered to be marginal for most air-data systems.

Data from reference 4 indicate the nulling error from the ball nose to be ±0.10° for dynamic pressures greater than 30 psf. Except for scatter in the data near $M_\infty = 1$, this value is supported by the present study, since the overall accuracy in the flight-test data would not have been possible with a larger nulling error. However, even the small value of ±0.10° can cause significant errors at the higher Mach numbers, as shown in figure 7(b). The estimated Mach number error due to nulling error at $M_\infty = 4$ is almost ±1.5 percent and increases to ±3.0 percent at M = 6. Larger nulling errors would cause excessive Mach number error.

Lip interference.– An unexpected, but interesting, facet of this investigation was the effect of the housing lip on the pressure at the 70° orifice (fig. 2). As angle of attack decreased, the lip increased the pressure, as shown in figure 8(a) for several Mach numbers. Figure 8(b) shows the approximate Mach number and angle-of-attack ranges in which lip interference was experienced. The range of interference began at about $\alpha = 10^\circ$ for a Mach number of 0.4 and decreased linearly to $\alpha = 0^\circ$ at a Mach number of 3.75.

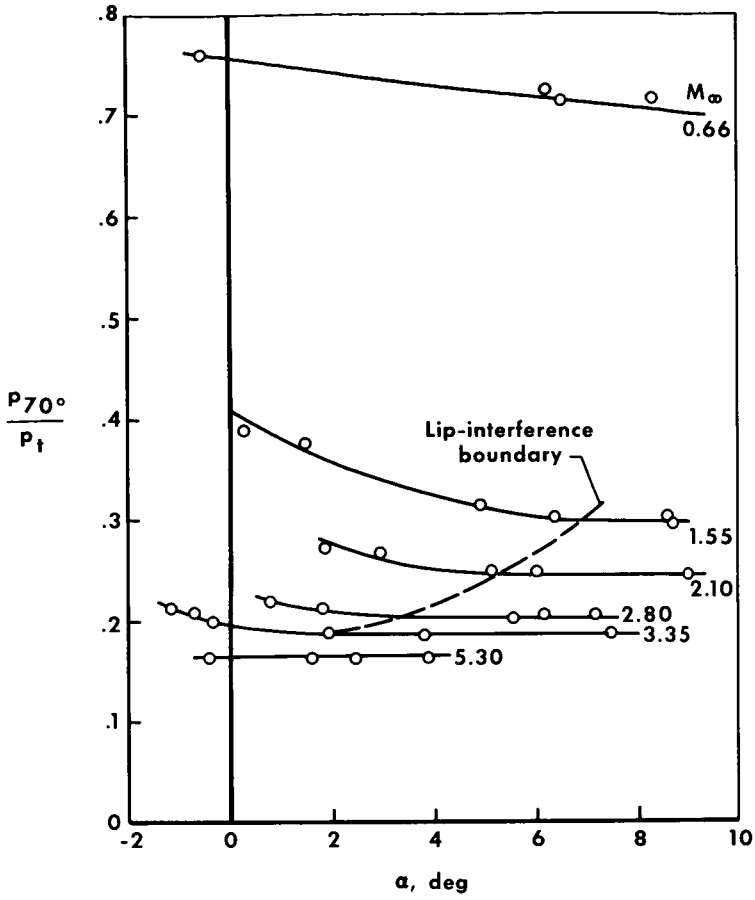

(a) Variation of pressure ratio with α for several Mach numbers.

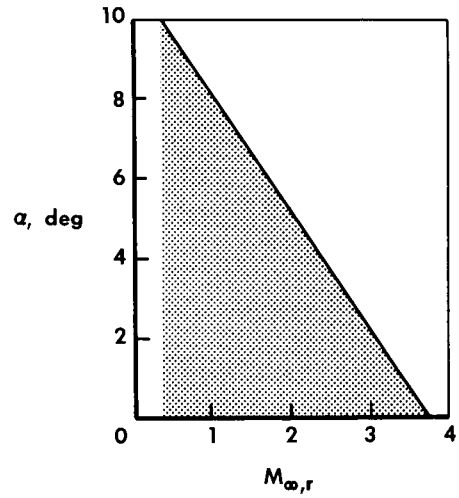

(b) Region of lip interference.

Flight data within this region were not used except at landing (M_∞ = 0.4 to 0.6) where valid data were difficult to obtain.

The percent error in Mach number caused by the lip in relation to angle of attack is shown in figure 8(c) for free-stream Mach numbers of 0.66, 1.55, 2.10, 2.80, and 3.35. Although the interference region is small for the higher Mach numbers, the shallow slope of the calibration curve (fig. 6(b)) results in a large Mach number error. Correspondingly, the interference region is large at the lower Mach

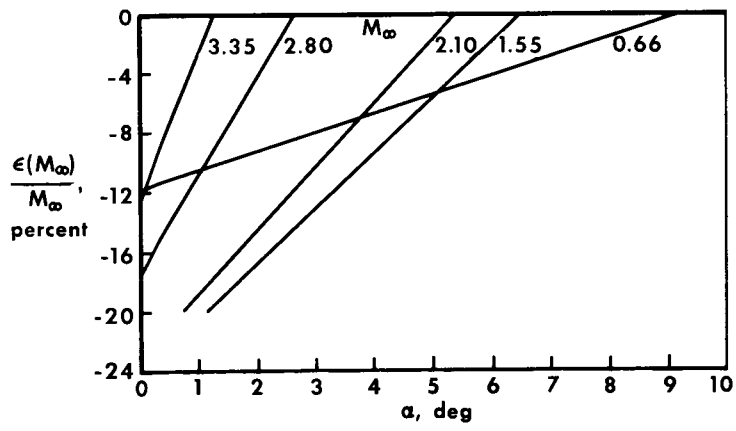

(c) Mach number error.

Figure 8.– Effects of lip interference.

numbers, but the Mach number error is small because of the relatively steep slope of the calibration curve. These errors make the system unacceptable for air-data use and can be eliminated only by removing the lip, since moving the orifice forward would tend to reduce the overall accuracy.

Comparison with other systems.— The probable error for the nose boom, ball nose, and the fuselage static pressure and ball-nose stagnation pressure is shown in figure 9. The curves represent percentage Mach number error due to data scatter about the faired calibration curve. It should be noted, however, that they do not represent position error. Probable error is defined by the Gauss error curve as being equal to or including 50 percent of the data points (ref. 6). The nose boom, used on the early X-15 flights, was more accurate than the other two systems. An internally recorded system using ball-nose stagnation pressure and static pressure from the fuselage was the least accurate. The error in this system would have been considerably lower if an angle-of-attack correction had been applied (see ref. 3).

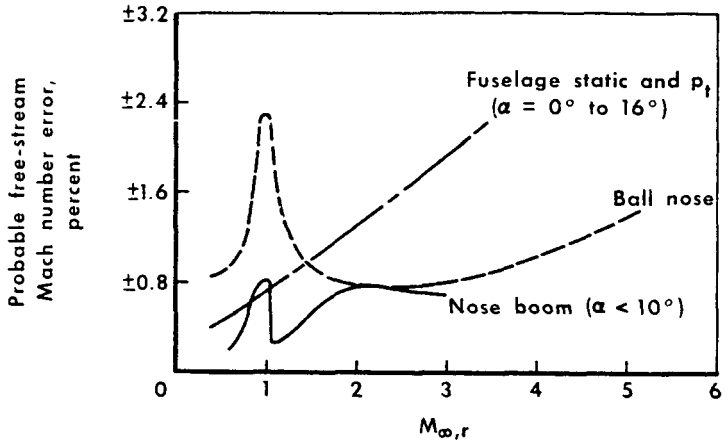

Figure 9.— Probable free-stream Mach number error for three X-15 air-data systems.

The probable error in Mach number for the modified ball nose is greater than ±1 percent in the transonic range and at Mach numbers greater than 3.8. The increasing error above $M_\infty = 2.5$ is due primarily to the flat slope of the calibration curve which is shown in figure 6(b). The sensor would be limited to low hypersonic speeds of about $M_\infty = 4.5$ because of the decreasing slope and the increasing influence of nulling error.

Static Pressure

Calibration.— Figure 10 shows calibration curves for determining pressure altitude in terms of the pressure ratios $\frac{p_{\infty,r}}{p_{70°}}$ and $\frac{p_{\infty,r}}{(p_t - p_{70°})}$ for reference free-stream Mach numbers extending to 5.3. A logarithmic scale was used to show the linearity of $\frac{p_{\infty,r}}{(p_t - p_{70°})}$ over the entire Mach number range. Modified Newtonian theory is included for comparison with the $\frac{p_{\infty,r}}{p_{70°}}$ curve and agrees fairly well with the flight-test data. Subsonically, $p_{70°}$ approaches $p_{\infty,r}$ in magnitude.

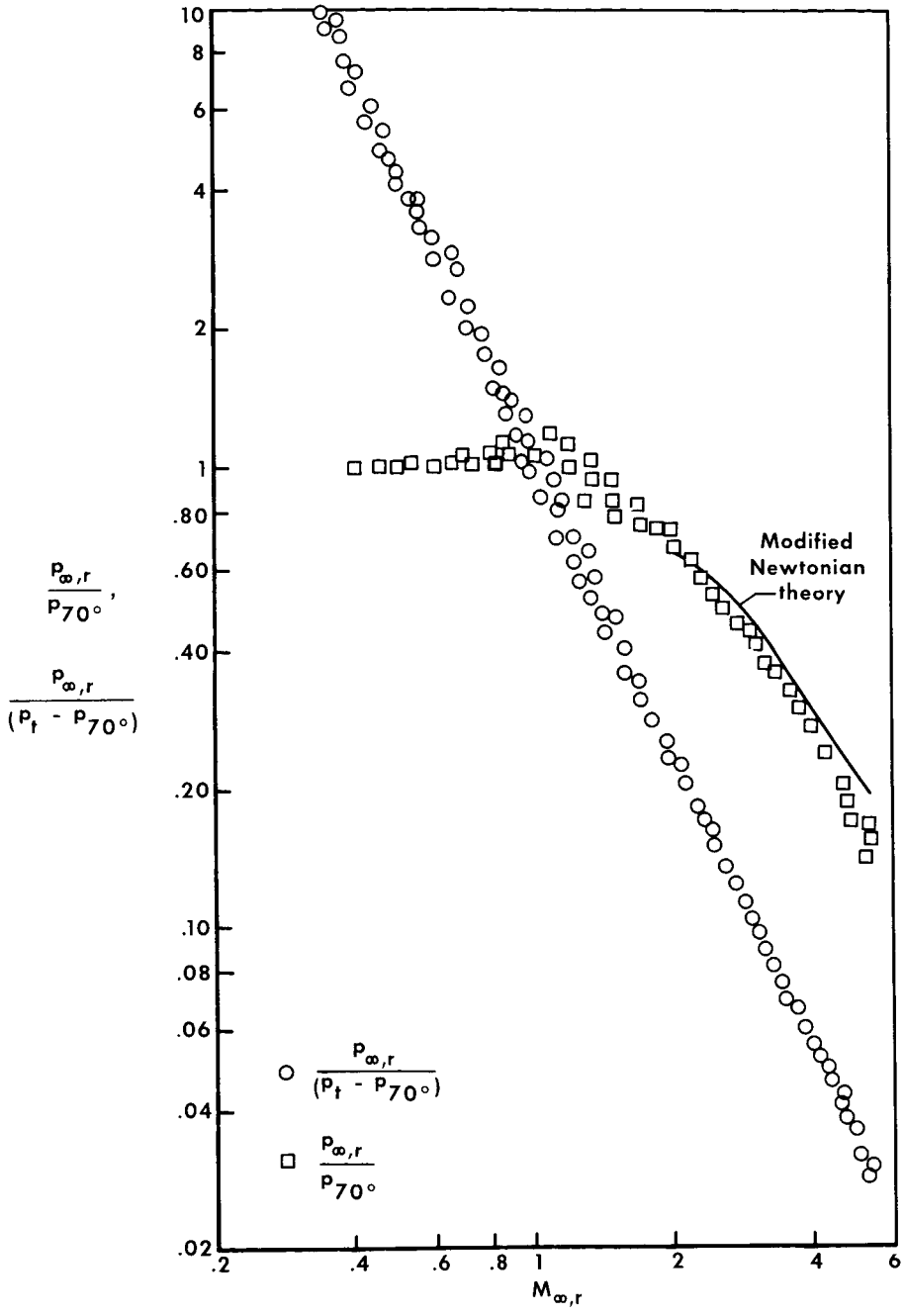

Figure 10.– Free-stream static pressure calibration.

Measurement error.– It was shown in equation (13) that the error in static pressure is a function of the error in $p_{70°}$ and Mach number. For the calibration curve based on 10 flights, the Mach number error from radar was assumed to be negligible. Thus, the only error remaining is the measurement error in $p_{70°}$, which was estimated as ±11.0 psf for the low-altitude

hookup and ±0.4 psf for the high-altitude hookup. Again, the flight-test data were not used when the estimated error in static pressure was greater than ±5 percent.

For an on-board air-data system, the second term of equation (13) becomes very important. Mach number is used in finding static pressure, so that any error in Mach number is carried over into the static-pressure calculation. If $\frac{\epsilon(p_{70°})}{p_{70°}}$ is assumed to be negligible in equation (13), a rapid and, in most cases, sufficiently accurate estimate of the error is

$$\frac{\epsilon(p_\infty)}{p_\infty} \approx 2\,\frac{\epsilon(M_\infty)}{M_\infty} \tag{15}$$

Dynamic Pressure

Figure 11 compares reference and ball-nose dynamic pressures up to q_∞ = 1,430 psf for a flight to M_∞ = 5.6. The ball-nose data agree well with reference measurements over the entire Mach number range; the difference at the maximum dynamic pressure was -30 psf for a 2.9 percent error.

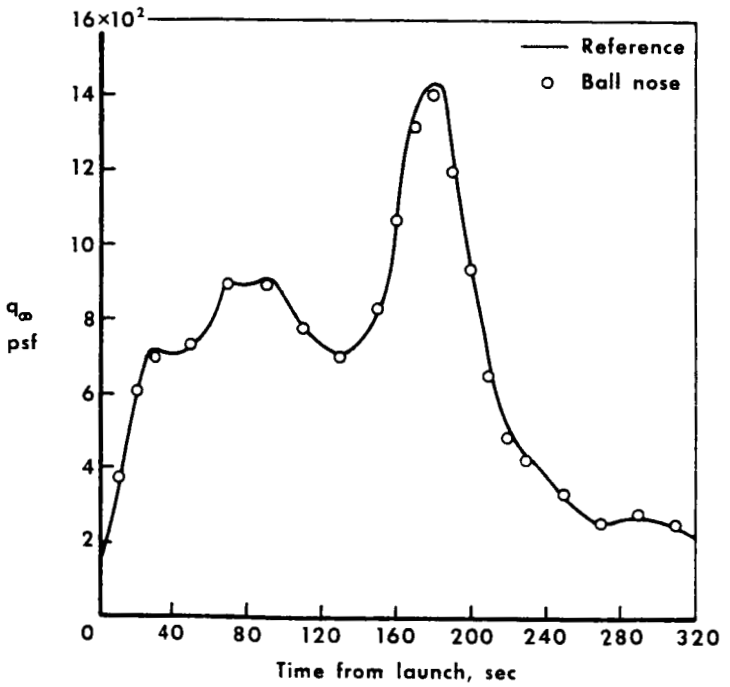

Figure 11.– Comparison of reference and ball-nose dynamic pressure for an X-15 flight.

Figure 12 shows the percent difference between ball-nose and reference dynamic pressure for three X-15 flights selected at random. (Data from one of the flights are shown in figure 11.) Scatter in the data is generally within ±3 percent and is consistently low at the higher values, perhaps as a result of ball-nose instrumentation problems. Accuracy decreases at the lower dynamic pressures because of the low measured pressures. The system is most accurate at high dynamic pressures where accuracy is critical for safety of flight.

X-15 "q" meter.– An on-board presentation of dynamic pressure was given to the X-15 pilot by the following equation

$$q_\infty = 0.53p_t \tag{16}$$

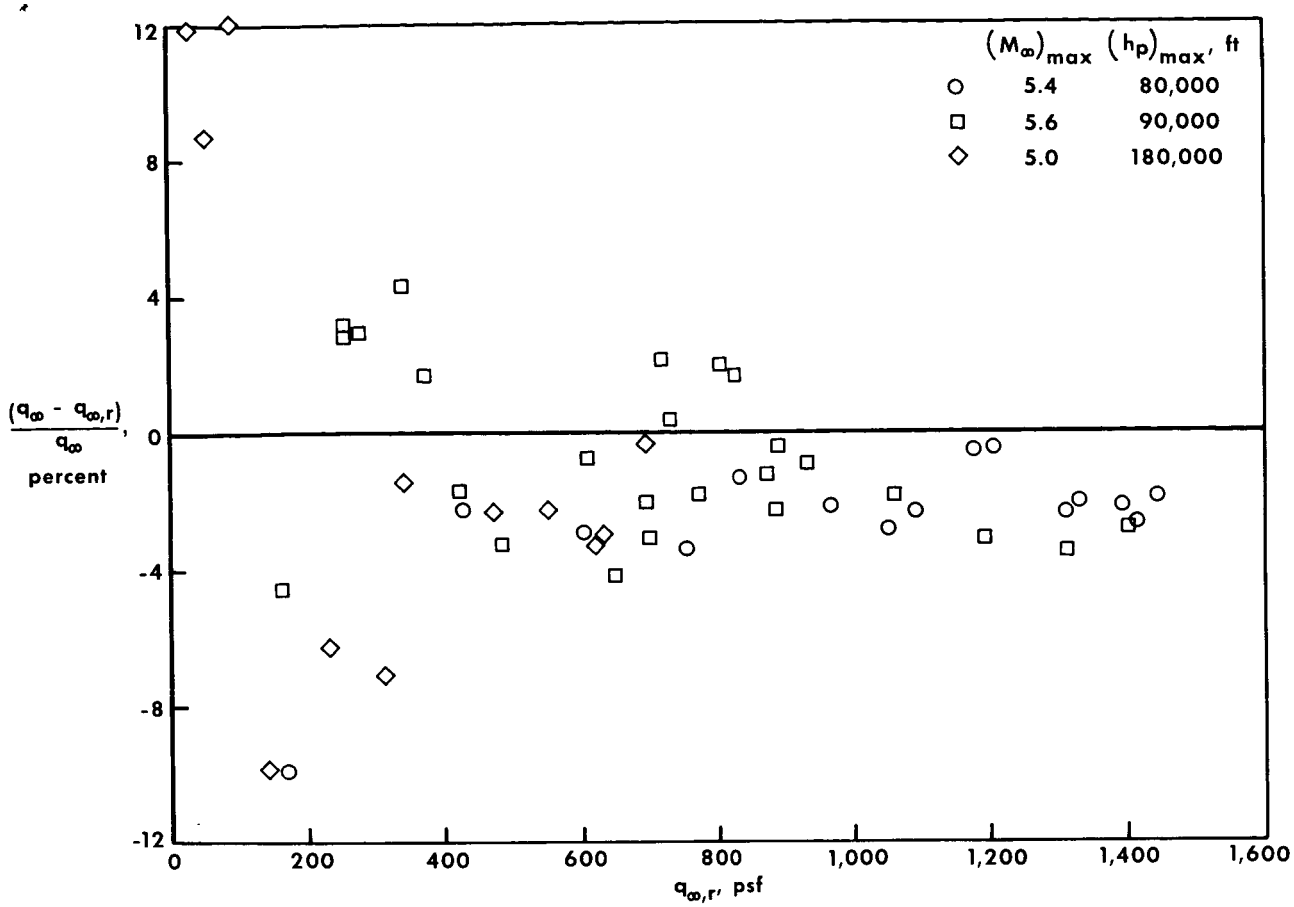

Figure 12.– Percent difference between ball-nose and reference dynamic pressures.

The constant, 0.53, was chosen as the value best suited to the X-15 speed range. The theoretical error which results from equation (16) is shown in figure 13 as a function of Mach number. Figure 13 also shows flight data obtained from cockpit movies of the "q" meter. The data agree well with theory; the scatter is attributed to measurement error. For free-stream Mach numbers greater than about 2.5, the "q" meter gave accurate readings of dynamic pressure which were determined independently of Mach number.

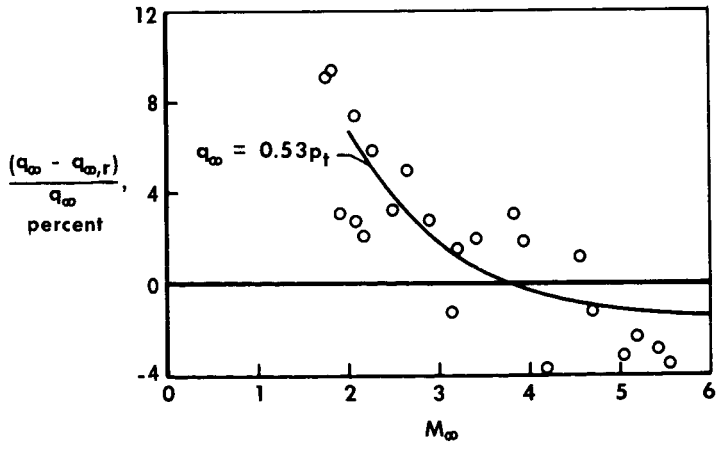

Figure 13.– Dynamic-pressure error using $q_\infty = 0.53p_t$.

CONCLUSIONS

Analysis of data recorded from a modified X-15 ball-nose flow-direction sensor led to the following conclusions:

1. The error in Mach number became excessive at Mach numbers greater than about 4.5 because of the flat slope of the calibration curve.

2. Mach number error, resulting from a constant nulling error, became proportionately larger with increasing Mach number.

3. For an on-board system, the percentage error in static pressure is about twice the percentage error in Mach number for free-stream Mach numbers greater than 2.

4. For an on-board presentation, the calculation of dynamic pressure from ball-nose stagnation pressure can be assumed independent of Mach number with good accuracy for free-stream Mach numbers greater than 2.5.

5. The sensor was unusable in the region of lip interference caused by the ball-nose housing junction.

Flight Research Center,
National Aeronautics and Space Administration,
Edwards, Calif., May 10, 1965.

REFERENCES

1. Hill, Jacques A. F.; Baron, Judson R.; Schindel, Leon H.; and Markham, John R.: Mach Number Measurements in High-Speed Wind Tunnels. AGARDograph 22, Oct. 1956.

2. Weil, Joseph: Review of the X-15 Program. NASA TN D-1278, 1962.

3. Larson, Terry J.; and Webb, Lannie D.: Calibrations and Comparisons of Pressure-Type Airspeed-Altitude Systems of the X-15 Airplane From Subsonic to High Supersonic Speeds. NASA TN D-1724, 1963.

4. Anon.: Q-Ball Airflow Direction and Air Data Sensors, General Descriptions. NORT 63-365, Nortronics, Div. of Northrop Corp., Oct. 1963.

5. Ames Research Staff: Equations, Tables, and Charts for Compressible Flow. NACA Rept. 1135, 1953. (Supersedes NACA TN 1428.)

6. Beers, Yardley: Introduction to the Theory of Error. Second ed., Addison-Wesley Pub. Co., Inc., 1962.

7. Inouye, Mamoru; and Lomax, Harvard: Comparison of Experimental and Numerical Results for the Flow of a Perfect Gas About Blunt-Nosed Bodies. NASA TN D-1426, 1962.

8. Kendall, James M., Jr.: Experiments on Supersonic Blunt-Body Flows. Progress Rept. No. 20-372 (Contract No. DA-04-495-Ord 18), Jet Propulsion Lab., Calif. Inst. Technol., Feb. 27, 1959.